Draft version February 2, 2008
Preprint typeset using LaTeX style emulateapj v. 5/14/03

arXiv:astro-ph/0411098v2 5 Apr 2005

THE STRÖMGREN SPHERE, THE ENVIRONMENT AND THE REIONIZATION IN THE LOCAL UNIVERSE OF THE HIGHEST REDSHIFT QSOS

Qingjuan Yu[1]
Department of Astronomy, 601 Campbell Hall, University of California at Berkeley, Berkeley, CA 94720

Youjun Lu
Department of Astronomy, 601 Campbell Hall, University of California at Berkeley, Berkeley, CA 94720;
Center for Astrophysics, University of Science and Technology of China, 96 Jinzhai Road, Hefei, Anhui 230026, P. R. China

Draft version February 2, 2008

ABSTRACT

In this paper we investigate the environment and reionization process around the highest redshift QSOs having Gunn-Peterson troughs ($z > 6.1$). Starting with the cosmic density perturbation and structure formation theory and the fact that the highest redshift QSOs are located in rare overdense regions, we show that the halo formation, gas distribution, and star formation around QSOs are biased from those of the cosmic average. We argue that a significant fraction of hydrogen in the Strömgren sphere around QSOs is ionized by photons from stars and that only about several percent to at most 10%–20% of the total hydrogen is left (e.g., in minihalos, halos, or high-density subregions) to be ionized by QSO photons. The cosmic average neutral hydrogen fraction at $z \sim 6.2-6.4$ should also be smaller than the upper limit of 10%–20% and may be only a few percent. We analyze the clumping property of the hydrogen ionized by QSOs and study the evolution of the Strömgren sphere. We find that the expected Strömgren radii from our models are consistent with observations if the lifetime of the highest redshift QSOs is about or longer than a few times 10^7 yr (as is the lifetime of the main population of QSOs; with comoving number density peaked at $z \sim$2–3). With such a QSO lifetime, the ages of most of the observed QSOs are long enough that the QSO photon emission is balanced by the recombination of the hydrogen ionized by QSO photons in their Strömgren spheres, and the expected Strömgren radii from the balance are independent of the detailed values of the QSO ages. We also point out a statistical method involving a larger sample of QSOs having Gunn-Peterson troughs in future observations, which may potentially check or rule out the possibility that the highest redshift QSOs have a shorter lifetime (e.g., $< 10^7$ yr), even without an accurate estimate of the hydrogen clumping property.

Subject headings: cosmology – theory: cosmology – early universe: galaxies – formation: galaxies: high redshift – quasars: general

1. INTRODUCTION

QSOs at redshifts $z > 6.1$ have been discovered by the Sloan Digital Sky Survey (SDSS) recently (Fan et al. 2001, 2003, 2004). Their spectra have shown the existence of the Gunn-Peterson absorption trough (Gunn & Peterson 1965; Scheuer 1965) at wavelengths blueward of the Lyα emission line, which suggests that hydrogen in the early universe is significantly neutral ($\gtrsim$ 1% in mass average; Becker et al. 2001; Djorgovski et al. 2001; Fan et al. 2001, 2002). Despite the presence of the Gunn-Peterson trough in the spectra, a significant amount of flux is transmitted at wavelengths blueward of but near the center of the Lyα line, which suggests that the regions surrounding these highest redshift QSOs are highly ionized by QSO photons (i.e., the proximity effect of QSOs, e.g., in Bajtlik et al. 1988). These highly ionized regions are generally idealized as spherical and called "Strömgren spheres." Their radii (or the Strömgren radii) can be estimated from the wavelength difference between the Gunn-Peterson trough and the Lyα line center (e.g.,White et al. 2003).

Physically the sizes of the highly ionized regions are closely related to not only the neutral hydrogen distribution in the local universe of these QSOs before their nuclear activities turn on but also the subsequent QSO luminosity evolution, either of which thus may be constrained by the Strömgren radii estimated from QSO spectra provided that the range of the other one is given. For example, using the observationally determined Strömgren radii and assuming the neutral hydrogen fraction (defined by the ratio of the neutral hydrogen number density to the total hydrogen number density) $x_{\rm HI} = 1$, Haiman & Cen (2002) found that the lifetime of one highest redshift QSO is not shorter than 2×10^7 yr (see also Pentericci et al. 2002) and White et al. (2003) got a substantially shorter lifetime for two; using the measured Strömgren radii of two highest redshift QSOs and some independent constraints on the QSO lifetime obtained by other studies, Wyithe & Loeb (2004a) argued that $x_{\rm HI}$ may be higher than tens of percent at $z \sim 6.3$, which is significantly higher than the lower limit of $x_{\rm HI} \gtrsim 1\%$ constrained by the flux upper limit of the Gunn-Peterson absorption trough (Becker et al. 2001; Fan et al. 2002; White et al. 2003). In addition, Cen & Haiman (2000) and Madau & Rees (2000) inves-

[1] Hubble Fellow
Electronic address: yqj,lyj@astro.berkeley.edu

tigated the structure of the transmitted spectra at wavelengths blueward of the Lyα line and pointed out that the red damping wing of the Gunn-Peterson trough might leave detectable features there (Miralda-Escudé 1998), which may also help to constrain $x_{\rm HI}$ (see a recent study by Mesinger et al. 2004 using mock data from simulations.

In most previous investigations on the reionization process around the highest redshift QSOs, the QSOs are implicitly assumed to be located in cosmic average regions. However, in the hierarchical formation and evolution scenario of galaxies and QSOs (e.g., Kauffmann & Haehnelt 2000), luminous QSOs (especially those at high redshifts $z > 6.1$) are located in rare overdense regions. The structure formation in these regions and consequently the gas distribution, star formation, and reionization of the neutral hydrogen may be significantly biased away from those in the regions with cosmic mean density. Some discussions in a few recent papers are also related to some biasing effects of a dense environment (e.g., Cen 2003b; Ciardi et al. 2003; Furlanetto et al. 2004; Gnedin & Prada 2004; Santos 2004; Wyithe & Loeb 2004b). The purpose of this paper is to quantitatively investigate the dense environment of the highest redshift QSOs, the reionization in their local universe due to ionizing photons from both stars and QSOs, and the evolution of their Strömgren spheres. Comparison of the expected Strömgren radii from the more realistic model with observations would improve our understanding of the universe's reionization history and the formation and evolution of QSOs.

This paper is organized as follows. The observational properties of the highest redshift QSOs that have the Gunn-Peterson trough are reviewed in § 2. In § 3, we investigate the environment around these QSOs in the framework of the cosmic density perturbation and structure formation theory (e.g., Lacey & Cole 1993). We first estimate how dense the environment is from the number density of the highest redshift QSOs. Then we introduce a hybrid model (see also Barkana & Loeb 2004) based on the excursion set approach of the Press-Schechter formula (Bond et al. 1991; Lacey & Cole 1993) to see how the structure or halo formation is enhanced in these rare overdense regions in § 3.2. Gas in halos may be shock heated, collisionally ionized, and then cool to form stars, galaxies, and/or QSOs. Ionizing photons from stars and QSOs will jointly contribute to the reionization of the surrounding neutral hydrogen. In this paper we isolate their effects and first consider the reionization due to stars (the variable $x_{\rm HI}$ in this paper represents the neutral hydrogen fraction obtained after considering the reionization due to stars but before the reionization due to the QSO becomes effective). The justification for this isolation is that before the cosmic time that the QSO redshift corresponds to, the QSO ionizing photon emission rate was high enough to be comparable to (or higher than) the ionizing photon emission rate from stars only in a short period (a few times $10^7\,{\rm yr}$) and the cumulative number of ionizing photons are mainly from stars (see detailed discussion in § 3.3 and 4.1). In § 3.3, using some simple star formation models, we find that more than 80%–90% of neutral hydrogen in these dense regions is ionized by photons from stars. Inhomogeneity or clumpiness of hydrogen may significantly affect the reionization process. In § 3.4 we give a rough estimate of the clumpiness of hydrogen ionized by QSO photons, based on the halo distribution obtained in § 3.2, some numerical simulation results obtained in other studies, and some physical arguments. In the environment of the highest redshift QSOs analyzed in § 3, we study the evolution of the apparent size of the Strömgren sphere highly ionized by QSO photons in § 4. The model results are compared with observations and the implications are discussed. The main conclusions are summarized in § 5.

Throughout this paper, we adopt a standard ΛCDM cosmological model with $\Omega_\Lambda = 0.73$, $\Omega_{\rm m} = 0.27$, $\Omega_{\rm b} = 0.0444$, $H_0 = 71\,{\rm km\,s^{-1}\,Mpc^{-1}}$, $\sigma_8 = 0.84$, and $n = 0.93$ (Spergel et al. 2003).

2. SAMPLE OF THE HIGHEST REDSHIFT QSOS THAT HAVE GUNN-PETERSON TROUGHS

To date, four QSOs have been observed at redshift $z > 6.1$, and all of them are detected to have the Gunn-Peterson trough in their spectra (Fan et al. 2003, 2004; White et al. 2003) and are compiled in Table 1. As seen from Table 1, the redshifts of the observed QSOs are in the range of $z_{\rm Q} \simeq$6.2–6.4. The redshift may be determined from the Lyα line (e.g., for SDSS J1623+3112; Fan et al. 2004), and the typical redshift error is ± 0.02, which is mainly caused by the uncertainty in the determination of the location of the line center in the spectra. The redshift of SDSS J1148+5251 is precisely determined from CO and $\rm Mg_{II}$ lines (Walter et al. 2003; Willott et al. 2003), and we simply assign a small error of ± 0.005 to its redshift (similarly for SDSS J1048+4637 whose redshift is determined by Mg_{II} line; Maiolino et al. 2004). Although the redshift of SDSS J1030+0524 has also been determined from metal lines (e.g., $\rm C_{IV}$), the redshift error can still be as large as 0.02, caused by the possible blueshift of the $\rm C_{IV}$ line (e.g., Richards et al. 2002), and we therefore set its redshift error to be $+0.02$ and -0.005. The Strömgren radii of three QSOs in Table 1 have been estimated through the difference between the QSO redshift and the redshift of the onset of the Lyα Gunn-Peterson trough in their spectra in the literature (i.e., $r^0_{\rm HII,obs}$; see also $z_{\rm HII,obs}$ in Tab. 1 for the corresponding redshift range of the Strömgren sphere, except for SDSS J1048+4637). The errors on $r^0_{\rm HII,obs}$ in Table 1 are introduced by the uncertainty in the determination of these QSO redshifts.

There may also exist uncertainties in the determination of the onset redshift of the Gunn-Peterson troughs, which further introduce uncertainties in the estimate of the Strömgren radii. For example, Mesinger & Haiman (2004) point out that the radius estimated through the Lyα trough may only give a lower limit of the Strömgren radius and that a better estimate may be obtained by using the Lyβ trough. Using the Lyβ trough and some numerical simulation results, Mesinger & Haiman (2004) increase the estimate of the Strömgren radius of SDSS J1030+0524 to $\sim 6\,{\rm Mpc}$ (from $\sim 4.6\,{\rm Mpc}$ listed in Tab. 1). Note that the new estimate might be affected by the numerical simulation used in the analysis (Mesinger & Haiman 2004), which does not well represent the overdense environment of the highest redshift QSOs discussed in this paper. In addition, other QSOs listed in Table 1 do not have the Strömgren radius estimated by using the Lyβ trough in the literature, and

thus we still mainly use the values estimated from the Lyα troughs for consistency in this paper and discuss the implication of a possible systematically larger value of the observational Strömgren radius in § 4.3.

We estimate the ionizing photon emission rates of these QSOs, $\dot{N}^0_{\rm phs,Q}$, by using their absolute magnitude M_{1450} at 1450 $\mathring{A}$ listed in Table 1 (compiled from Fan et al. 2001, 2003, 2004) and the spectral templates of relatively low redshift QSOs ($z \lesssim 3$) shown in Telfer et al. (2002). (Fan et al. 2004 have found that the average spectrum of the highest redshift QSOs is similar to that in Telfer et al. 2002.) In Telfer et al. (2002), the average spectra of the low-redshift QSOs (energy radiated per unit time and per logarithmic interval of frequency $\nu f_\nu \propto \nu^{1+\alpha}$) is well fitted by a double power law in the optical to EUV band. For radio-loud QSOs, the EUV and near-UV spectral indices are $\alpha_{\rm EUV} = -1.96 \pm 0.12$ and $\alpha_{\rm NUV} = -0.67 \pm 0.08$, respectively, with the break at $\sim 1280\mathring{A}$, while for radio-quiet QSOs they are $\alpha_{\rm EUV} = -1.57 \pm 0.17$ and $\alpha_{\rm NUV} = -0.72 \pm 0.09$, respectively. We count photons with energy in the range 13.6–54.4 eV as ionizing photons. Since so far little information on the radio properties of the highest redshift QSOs is available, we obtain two emission rates for each QSO listed in Table 1, the smaller of which is obtained by adopting the spectral indices of radio-loud QSOs and the larger of which is obtained by adopting the spectral indices of radio-quiet QSOs. We take the middle point of the whole range of the two values (including their errors) as $\dot{N}^0_{\rm phs,Q}$ and take the whole range as the error range of $\dot{N}^0_{\rm phs,Q}$ (see also the filled circles and their horizontal error bars in Fig. 3a). Note that for SDSS J1030+0524, compared to the rate listed in Table 1, a substantially smaller rate is obtained in Mesinger & Haiman (2004) by fitting the spectrum of the QSO in a surrounding hydrogen density distribution given by a numerical simulation. As mentioned above, the numerical simulation used in Mesinger & Haiman (2004) mimics the cosmic average environment rather than the rare overdense environment around the highest redshift QSOs; thus the smaller rate may be an underestimate since more ionizing photons would be required to balance the recombination in a denser environment.

The highest redshift QSOs are extremely rare and their comoving number density $N_{\rm Q}$ is roughly the same as the density of the QSOs with absolute magnitude $M_{1450} < -26.7$ at $z \sim 6$ estimated by Fan et al. (2003, 2004), i.e., $N_{\rm Q} \simeq (6 \pm 2) \times 10^{-10}\,{\rm Mpc}^{-3}$. (Note that the value of $N_{\rm Q}$ is obtained by assuming a cosmological model with $H_0 = 65\,{\rm km\,s^{-1}\,Mpc^{-1}}$, $\Omega_{\rm m} = 0.35$, and $\Omega_\Lambda = 0.65$; we have adjusted this value to the cosmological model adopted in this paper and found no significant difference.)

3. THE ENVIRONMENT AROUND THE HIGHEST REDSHIFT QSOS

The highest redshift QSOs are located in rare overdense regions according to current structure and QSO formation and evolution picture in the ΛCDM cosmogony (e.g., Kauffmann & Haehnelt 2000). To quantify the environment of these QSOs, we first estimate the mean mass overdensity in their surrounding regions in § 3.1. Then we study the structure and halo formation in these overdense regions in § 3.2, and study the star formation and the reionization due to ionizing photons emitted from these stars in § 3.3. In § 3.4 we study the clumpiness of hydrogen in the Strömgren sphere of the QSOs.

3.1. *Overdensity*

The mean overdensity within a sphere with proper radius r at redshift z is defined by $\bar{\delta}_r \equiv [\langle\rho\rangle_r - \bar{\rho}]/\bar{\rho}$, where $\langle\rho\rangle_r$ is the average comoving mass density in the sphere and $\bar{\rho}$ is the comoving cosmic mean mass density. We denote the comoving radius of the sphere by $R = r(1+z)$. (Here we do not distinguish the difference between the Eulerian radius and the Lagrangian radius, since the overdensity considered in this paper is small.) The variance of the density fluctuations at redshift z in spheres with comoving radius R, $\sigma^2(R,z)$, can be determined by (e.g., see eq. 2.55 in White 1994)

$$\sigma^2(R,z) = D^2(z) \int_0^\infty \frac{dk}{2\pi^2} k^2 P(k) W^2(kR), \qquad (1)$$

where $D(z)$ is the linear growth factor of perturbations at z and normalized to 1 at the present time, $P(k)$ is the power spectrum of the density perturbation field and is computed with the fitting formula of Eisenstein & Hu (1999), and $W(kR) = 3[\sin(kR) - kR\cos(kR)]/(kR)^3$ is the top-hat window function. If the perturbations on the scale of r are still in the linear growth regime at redshift z, the mean overdensity $\bar{\delta}_r$ follows a Gaussian distribution:

$$p(\bar{\delta}_r, z) d\bar{\delta}_r = \frac{1}{\sqrt{2\pi}\sigma(R,z)} \exp\left[-\frac{\bar{\delta}_r^2}{2\sigma^2(R,z)}\right] d\bar{\delta}_r, \qquad (2)$$

and the probability that a random region with scale r has a mean overdensity higher than a value $\bar{\delta}'_r$ is given by

$$\mathcal{P}(>\bar{\delta}'_r, z) = \int_{\bar{\delta}'_r}^\infty p(\bar{\delta}_r, z) d\bar{\delta}_r. \qquad (3)$$

Since the Strömgren radii measured from the observed QSO spectra are around 5 Mpc, below we consider a sphere with proper radius $r_{\rm Q} = 5\,{\rm Mpc}$. According to equation (1), the standard deviation of the density fluctuations in this sphere at $z \simeq 6$ is $\sigma[R = r_{\rm Q}(1+z), z \simeq 6] \simeq 0.06$, which is much smaller than the critical overdensity $\delta_c = 1.68$ for dynamical collapse, and the perturbations are still in the linear growth regime. Thus equations (2) and (3) can be applied to these spheres.

In regions with sufficiently high overdensity, sufficiently massive halos will form and these halos are the hosts of luminous QSOs. In a random spherical region with proper radius $r_{\rm Q} = 5\,{\rm Mpc}$ at $z \sim 6$, the probability of finding a halo capable of hosting nuclear-active QSOs with $M_{1450} < -26.7$ (e.g., with mass $\sim 10^{13}\,{\rm M}_\odot$) is

$$f_{\rm duty}^{-1} N_{\rm Q} \frac{4\pi}{3} [r_{\rm Q}(1+z)]^3 \simeq 1.0 \times 10^{-4} f_{\rm duty}^{-1}, \qquad (4)$$

where $f_{\rm duty}(z)$ represents the duty cycle of QSOs, defined to be the number ratio of the nuclear active QSOs to the halos capable of hosting the QSOs at redshift z. The halos capable of hosting QSOs include both those hosting a nuclear-active QSO and those hosting a dead QSO with nuclear activity quenched. For the highest redshift

QSOs, we simply assume $f_{\rm duty} \sim 1$ because most sufficiently massive halos (e.g., $\gtrsim 10^{13}\,{\rm M}_\odot$) at $z \sim 6$ are actually formed within a period (from $z = 7$ to 6; e.g., see Fig. 1 in Mo & White 2002) not significantly longer than the QSO lifetime ($>$ a few times 10^7 yr; Yu & Lu 2004a; Yu & Tremaine 2002; see more discussions about the QSO lifetime in § 4). By multiplying equation (3) by a factor of 2 (this factor comes from the so-called cloud-in-cloud problem; see discussions in Bond et al. 1991) and then setting it equal to equation (4), we obtain that the mean overdensity of the regions associated with the highest redshift QSOs is $\bar{\delta}_{r_{\rm Q}} \geq \bar{\delta}'_{r_{\rm Q}} \sim 4\sigma(R, z \simeq 6) \simeq 0.25$. Since the overdensity distribution $g(\bar{\delta}_r)$ decreases exponentially at the high overdensity end, most of these overdense regions associated with the highest redshift QSOs do not have a mean overdensity significantly higher than $\bar{\delta}'_{r_{\rm Q}}$, but near the value.

Note that the connection of equation (3) with equation (4) above has assumed a one-to-two correspondence between the likelihood of finding a region with mean overdensity above a certain value and the likelihood of a same-sized region containing a halo capable of hosting a quasar. Although in principle there might exist regions with overdensity above the certain value but not containing such a halo, the simple approach above is good enough in practice for the rare overdense regions and for the purpose of this paper. For example, given a halo with a certain mass, the method in Barkana (2004; for simplicity the details are not presented here), which is also based on the (extended) Press-Schechter formalism, may provide the expected average overdensity within a certain region around the halo and the standard deviation of the overdensity. Assuming that the host halos of the highest redshift QSOs are around $10^{13}\,{\rm M}_\odot$ (or $2 \times 10^{13}\,{\rm M}_\odot$) and using the method in Barkana (2004), we obtain an average overdensity of ~ 0.13 (or 0.16) within the region with radius $r_{\rm Q}$ surrounding the halo, which is smaller than the estimate above. Hereafter, we simply adopt $\bar{\delta}_{r_{\rm Q}} = \bar{\delta}'_{r_{\rm Q}} \simeq 0.25$ as the mean overdensity of the spheres with proper radius $r_{\rm Q} = 5\,{\rm Mpc}$ centering on the highest redshift QSOs. Using the value of $\bar{\delta}_{r_{\rm Q}} = 0.13$ will not qualitatively affect the conclusions in this paper.

3.2. *The formed structure*

In this section, we introduce a hybrid model to estimate the mass distribution of halos formed in the rare overdense regions associated with the highest redshift QSOs (see also Barkana & Loeb 2004).

We define the halo mass function as $\frac{dN}{dM}(z)$ so that $\frac{dN}{dM}dM$ represents the comoving number density of halos with mass in the range $M \rightarrow M + dM$ at redshift z. In the cosmic average regions, the halo mass function can be given by

$$\frac{dN}{dM} = \frac{\bar{\rho}}{M}\left|\frac{d\sigma^2(R_c, z)}{dM}\right| f[\delta_c, \sigma^2(R_c, z)], \qquad (5)$$

where $R_c = (3M/4\pi\bar{\rho})^{1/3}$, and $f[\delta_c, \sigma^2(R_c, z)]d\sigma^2(R_c, z)$ is the mass fraction of halos with mass in the range $M \rightarrow M+dM$ at redshift z. In the model of Press & Schechter (1974), $f[\delta_c, \sigma^2(R_c, z)]$ is given by

$$f_{\rm PS}[\delta_c, \sigma^2(R_c, z)] = \frac{1}{\sqrt{2\pi}}\frac{\nu}{\sigma^2(R_c, z)}\exp(-\frac{\nu^2}{2}), \qquad (6)$$

where $\nu = \delta_c/\sigma(R_c, z)$. Compared to the results obtained from cosmological simulations with very large volumes, however, the Press-Schechter mass function substantially underestimates the abundance of the rare massive halos that host galaxies at high redshifts and overestimates the abundance of intermediate-mass halos. To more accurately match the simulation results, Sheth & Tormen (1999) introduce a new formula

$$f_{\rm ST}[\delta_c, \sigma^2(R_c, z)] = \frac{A'}{\sqrt{2\pi}}\frac{\sqrt{a'}\nu}{\sigma^2(R_c, z)}\left[1 + \frac{1}{(a'\nu^2)^{q'}}\right]\exp\left(-\frac{a'\nu^2}{2}\right) \qquad (7)$$

with the best-fit parameters $a' = 0.707$ and $q' = 0.3$, and the normalization parameter $A' = 0.322$. This formula can be derived by introducing an ellipsoidal collapse model instead of the usually adopted spherical collapse model into the excursion set approach of the Press-Schechter formula (Sheth et al. 2001). In the model of Sheth & Tormen (1999), we have the cosmic average mass fraction of halos with mass higher than M given by

$$F_{\rm ST,halo}(> M, z) = \int_{\sigma^2(R_c,z)}^{\infty} f_{\rm ST}(\delta_c, \sigma^2)d\sigma^2. \qquad (8)$$

In a rare overdense region with volume much smaller than the universe, the halo mass distribution significantly deviates from the cosmic mean distribution shown by equations (5)-(7). Similar to using the excursion set approach to get the extended Press-Schechter formula (Bond et al. 1991; Lacey & Cole 1993), we have the corresponding biased mass fraction of $f_{\rm PS}[\delta_c, \sigma^2(R_c, z)]$ in a region with comoving radius R and mean overdensity $\bar{\delta}_r$ at redshift z given by

$$f_{\rm PS}^{\rm bias}[\delta_c, \sigma^2(R_c, z); \bar{\delta}_r, R] = f_{\rm PS}[\delta_c - \bar{\delta}_r, \sigma^2(R_c, z) - \sigma^2(R, z)], \qquad (9)$$

and the mass fraction of halos with mass higher than M given by

$$F_{\rm PS,halo}^{\rm bias}(> M, z) = {\rm erfc}\left(\frac{\delta_c - \bar{\delta}_r}{\sqrt{2[\sigma^2(R_c, z) - \sigma^2(R, z)]}}\right). \qquad (10)$$

As shown in Barkana & Loeb (2004), the halo mass function in overdense regions can be obtained by adjusting the Sheth-Tormen formula with a relative correction based on the extended Press-Schechter model (Bond et al. 1991; Lacey & Cole 1993), which can match cosmological simulation results well. Similar to this hybrid model, the biased halo mass function in the regions with mean overdensity $\bar{\delta}_r$ can be obtained by[2]

$$\left[\frac{dN}{dM}\right]^{\rm bias} = \frac{(1 + \bar{\delta}_r)\bar{\rho}}{M} \times \left|\frac{d\sigma^2(R_c, z)}{dM}\right| f^{\rm bias}[\delta_c, \sigma^2(R_c, z); \bar{\delta}_r, R], \qquad (11)$$

[2] The biased halo mass function in a high-density region may also be obtained by using the ellipsoidal collapse moving barrier model in Sheth & Tormen (2002) instead of the hybrid model used here.

where

$$f^{\rm bias}[\delta_c,\sigma^2(R_c,z);\bar{\delta}_r,R]=f_{\rm ST}[\delta_c,\sigma^2(R_c,z)] \times\frac{f^{\rm bias}_{\rm PS}[\delta_c-\bar{\delta}_r,\sigma^2(R_c,z)-\sigma^2(R,z)]}{f_{\rm PS}[\delta_c,\sigma^2(R_c,z)]}. \quad (12)$$

In these overdense regions, the mass fraction of halos with mass higher than M is given by

$$F^{\rm bias}_{\rm halo}(>M,z)= \int_{\sigma^2(R_c,z)}^{\infty} f^{\rm bias}(\delta_c,\sigma^2;\bar{\delta}_r,R)d\sigma^2. \quad (13)$$

In halos with sufficiently high masses, most of the gas in them is collisionally ionized and some of the ionized gas may cool to form stars, galaxies, and/or QSOs. Neutral hydrogen in the universe may then be photoionized by photons from stars and QSOs. We define a characteristic mass scale $M_{\rm min}$, the minimum mass of halos whose potentials are deep enough to retain ionized gas in the photoionization equilibrium. The temperature of ionized gas in photoionization equilibrium is $\simeq 10^4$ K, and we have $M_{\rm min}=3.4\times10^7\,{\rm M}_\odot[10/(1+z)]^{1.5}$ (see details for the determination of this mass scale in Appendix B in Benson et al. 2001). We include both the gas outside halos with mass greater than $M_{\rm min}$ and that inside these halos but not collisionally ionized as IGM (the mass of baryons in galaxies is negligible; see Fig. 1 below). In these regions, the mass fraction of hydrogen that is in IGM is given by

$$x_{\rm H,IGM}(z)= 1-\int_{M_{\rm min}}^{\infty} y_{\rm H}\frac{M}{(1+\bar{\delta}_r)\bar{\rho}}\left[\frac{dN}{dM}\right]^{\rm bias}dM, \quad (14)$$

where $y_{\rm H}$ is the fraction of hydrogen that is collisionally ionized in a halo with mass M at the virial temperature $T_{\rm vir}$, and the ratio of the baryonic mass to the total mass in halos is assumed to be the same as the cosmic mean $\Omega_{\rm b}/\Omega_{\rm m}$. The virial temperature is $T_{\rm vir}=\frac{\mu m_{\rm H}}{2k_B}\frac{GM}{r_{\rm vir}}$, where $\mu\sim0.6$ is the mean molecular weight, $m_{\rm H}$ is the proton mass, k_B is the Boltzmann constant, and $r_{\rm vir}$ is the virial radius of the halo (see, e.g., Barkana & Loeb 2001). The determination of the detailed distribution of collisionally ionized hydrogen (see also eq. 20 below) would need to take into account detailed gas dynamics inside the halos (e.g., photo-evaporation processes, dynamics related to galactic disks), which is currently not well understood. The $y_{\rm H}$ used in this paper comes from Sutherland & Dopita (1993), as commonly adopted.

Our calculation shows that in the rare overdense regions associated with the highest redshift QSOs, $x_{\rm H,IGM}(r_{\rm Q},z_{\rm Q}\simeq6.2-6.4)\simeq0.88-0.89$ while the cosmic mean $\bar{x}_{\rm H,IGM}(z_{\rm Q})$ is around 0.94.

3.3. *The reionization due to stars*

Star formation in the formed halos is directly related to the cooling of their virialized gas due to radiation by atomic, molecular, or metal lines. Gas cooling due to atomic lines, and thus star formation, can be very efficient in halos with $T_{\rm vir}>10^4$ K, as usually argued (e.g., Hernquist & Springel 2003). However, atomic line cooling is not efficient in halos with $T_{\rm vir}<10^4$ K (the so-called minihalos). Molecular hydrogen (H_2) line cooling may be important for the very first (Population III) star formation in those minihalos at very high redshift (e.g., $z>10$; see Abel et al. 2002; Bromm et al. 1999). These Population III stars may lead to the reionization of the universe at very high redshift, but this may be unimportant for the (second) reionization that finished at $z\sim6$ (Cen 2003a). At lower redshift, external UV radiation may suppress the molecular H_2 abundance in those minihalos and thus reduce the cooling due to H_2 lines (e.g., Haiman et al. 1996). However, the precise cooling threshold and H_2 abundance in these regimes are not well known. Furthermore, star formation in minihalos is also likely to be suppressed by the processes of photoevaporation and supernova disruption. Below we only consider star formation in halos with $T_{\rm vir}>10^4$ K and neglect star formation in minihalos. Detailed physical processes of star formation in halos with $T_{\rm vir}>10^4$ K are complicated and not fully understood. Here we adopt two simple models to estimate how many baryons form stars in these halos:

- Model (a): The star formation efficiency (i.e., the mass fraction of baryons to form stars) in halos is assumed to be independent of the halo mass, as adopted in Cen (2003a). To satisfy the constraint that the reionization epoch ends at $z\sim6$, Cen (2003a) obtained a best-fit value of 0.1 for the star formation efficiency in halos with a virial temperature greater than 10^4 K. We adopt this value and thus have the mass fraction of baryons that are in formed stars in the rare overdense regions associated with the highest redshift QSOs, $g^{\rm bias}_{\rm star}(z)\simeq0.1F^{\rm bias}_{\rm halo}(>M_4,z)$, where M_4 is the mass of halos with virial temperature of 10^4 K.

- Model (b): the star formation efficiency is assumed to depend on the halo mass. After considering the feedback due to galactic winds in the star formation process, Hernquist & Springel (2003) argued that the normalized star formation rate (the mass fraction of baryons to form stars per unit time) may maintain a roughly constant level for halos with virial temperatures in the range 10^4-$10^{6.5}$ K but may rise to a level approximately 3 times higher for halos with hotter virial temperatures. Based on this approximation, the star formation rate in halos with temperature $T_{\rm vir}$ is given by (see eqs. 41, 43 and more details in Hernquist & Springel 2003)

$$S(T_{\rm vir},z)\simeq \begin{cases} s_0q(z) & \text{for } 10^4{\rm K}<T_{\rm vir}<10^{6.5}{\rm K},\\ 3s_0q(z) & \text{for } T_{\rm vir}>10^{6.5}{\rm K},\\ 0 & \text{otherwise,}\end{cases} \quad (15)$$

where $q(z)=\left[\frac{\tilde{\chi}\chi}{(\tilde{\chi}^m+\chi^m)^{1/m}}\right]^{9/2\eta}$, $\chi=[\Omega_{\rm m}(1+z)^3+\Omega_\Lambda]^{1/3}$, $m=6$, and $\eta=1.65$. For the cosmological model adopted in this paper, we adjust $\tilde{\chi}$ from 4.6 to 4.4 and s_0 from $0.006h$ Gyr^{-1} to $0.008h$ Gyr^{-1} (see details for the dependence of $\tilde{\chi}$ and s_0 on cosmological parameters in Hernquist & Springel 2003). Thus the mass fraction of baryons that are in formed stars in the rare overdense regions associated with the highest redshift QSOs is given by

$$g^{\rm bias}_{\rm star}(z)\simeq\int_z^\infty s_0q(z)\times$$

$$[F_{\rm halo}^{\rm bias}(>M_4,z)+2F_{\rm halo}^{\rm bias}(>M_{6.5},z)]\frac{dt}{dz}dz, \quad (16)$$

while the corresponding cosmic mean is given by

$$\bar{g}_{\rm star}(z)\simeq\int_z^\infty s_0 q(z)\times$$

$$[F_{\rm ST,halo}(>M_4,z)+2F_{\rm ST,halo}(>M_{6.5},z)]\frac{dt}{dz}dz, \quad (17)$$

where $M_{6.5}$ is the mass of a halo with virial temperature $10^{6.5}$ K.

We plot the results of $g_{\rm star}^{\rm bias}(z)$ and $\bar{g}_{\rm star}(z)$ in Figure 1 for both models a and b. Their values at the QSO redshift $z_{\rm Q}\simeq 6.2-6.4$ are summarized in Table 2. As seen from Figure 1, both models indicate that star formation in the overdense regions (*solid line*) is significantly biased away from or higher than the cosmic average at the same redshift (*dashed line*). Although the mass fractions of baryons in formed stars obtained from models a and b are not exactly the same, the two models give a consistent result in that the mass fraction of baryons in formed stars in the regions associated with the highest redshift QSOs at $z_{\rm Q}\sim 6.2-6.4$ is similar to the corresponding cosmic mean values at a later time $z\sim 5$, i.e., $g_{\rm star}^{\rm bias}(z_{\rm Q})\simeq\bar{g}_{\rm star}(z\sim 5)$ (indicated by the arrows in Fig. 1; see also Tab. 2). Since the number of ionizing photons emitted from stars is proportional to the mass of baryons in formed stars, the cumulative number of the ionizing photons produced in the stars in the rare overdense regions associated with the highest redshift QSOs at $z_{\rm Q}\sim 6.2-6.4$ is thus similar to that of the corresponding cosmic mean at a later time $z\sim 5$. However, their hydrogen ionization statuses may not be naively similar, for example, because of differences in their proper densities or in the process/time for hydrogen to dynamically respond to the ionization (especially for the photo-evaporation process of minihalos).

We assume the initial mass function for star formation in the surrounding regions of the highest redshift QSOs is similar to that measured in the nearby universe (Scalo 1998) and thus that roughly 4000 ionizing photons are produced per baryon in the formed stars (e.g., Barkana & Loeb 2001). The rate of ejection of the ionizing photons into the IGM can be given by

$$\dot{N}_{\rm phs,star}^{\rm bias}\simeq\frac{4\pi}{3}R^3(1+\bar{\delta}_r)N_{\rm b}\frac{dg_{\rm star}^{\rm bias}(z)}{dt}\times 4000 f_{\rm esc}, \quad (18)$$

where $N_{\rm b}$ is the baryon comoving number density and $f_{\rm esc}$ is the fraction of the ionizing photons escaping into the IGM and is roughly in the range 0.1-0.2 (e.g., Cen 2003a). In spheres with proper radius $r_{\rm Q}=5\,{\rm Mpc}$ associated with the highest redshift QSOs, we obtain $\dot{N}_{\rm phs,star}^{\rm bias}(z_{\rm Q})$ for both models a and b and list them in Table 2. For comparison, the cosmic mean injection rate of ionizing photons due to stars at $z\sim 5$ in the same comoving volume, $\bar{\dot{N}}_{\rm phs,star}\simeq\frac{4\pi}{3}R^3N_{\rm b}\frac{d\bar{g}_{\rm star}(z)}{dt}\times 4000 f_{\rm esc}$, is also listed in Table 2, which is roughly half of $\dot{N}_{\rm phs,star}^{\rm bias}(z_{\rm Q})$. Assuming that the background ionizing energy intensity J_ν (ν: photon frequency) is mainly contributed by stars, we estimate that an ionizing photon emission rate of $\bar{\dot{N}}_{\rm phs,star}$ leads to the background intensity J_{-21} at the Lyman limit in units of 10^{-21}ergs cm^{-2} s^{-1} Hz^{-1} sr^{-1} of about 0.06-0.13 for model a and 0.1-0.2 for model b (using eq. 29 in Madau et al. 1999). These numbers are roughly consistent with those determined from observations at $z\sim 5$ (see Fig. 2 in Fan et al. 2002), which suggests that the star formation models used in this paper are roughly consistent with observations. In the rare overdense regions around the highest redshift QSOs, according to equation (18) the cumulative number of the ionizing photons emitted from stars before $t(z_Q)$ is about 5-10 per hydrogen atom in the IGM within the Strömgren sphere, which is substantially higher than that from the central QSO ($\lesssim 1-2$; see also discussion in § 4.1).

As shown above, a large number of stars have already formed in the rare high-density regions before $z\sim 6$, and in most of the time before the cosmic time $t(z_{\rm Q})$, stars are the main sources of the ionizing photons contributing to the re-ionization of neutral hydrogen in the IGM (as mentioned in the introduction and as will also be discussed in § 4.1). The reionization starts in low-density regions (or voids) and then gradually penetrates deeper into high-density regions (see discussions in Gnedin 2000; Miralda-Escudé et al. 2000). Thus, before the reionization by the QSO photons becomes effective, the IGM in low-density regions surrounding those stars (or galactic units) has already been highly ionized, while the IGM in high-density regions may still be significantly neutral since the ionizing photons from stars are still insufficient to ionize all the IGM. The division from the highly ionized regions to the significantly neutral regions may be characterized by a critical overdensity $\Delta_{\rm crit}$, where the overdensity Δ is defined through $\Delta\equiv\rho_b/\bar{\rho}_b$, ρ_b is the comoving baryon mass density at a given space position, and $\bar{\rho}_b$ is the cosmic comoving mean mass density of baryons (note the difference from the definition of the overdensity $\bar{\delta}_r$, which is averaged over a proper scale of r). After the nuclear activity of the QSO turns on and the emission of its ionizing photons becomes significant, QSO photons will ionize some remaining neutral hydrogen (in high-density regions) not ionized by stars. Compared to ionizing photons from stars, the photons from QSOs are much harder and can penetrate into high-density regions more deeply. In addition, QSOs are rare point sources located in high-density regions, while stars are embedded in relatively numerous halos and act like diffuse sources. A significant fraction of the ionizing photons from stars may leak out of the regions (with $r_{\rm Q}=5\,{\rm Mpc}$) considered in this paper, while ionizing photons from QSOs do not, but are absorbed.

Here we give a rough estimate of the ionization status due to stars in the overdense regions associated with the highest redshift QSOs, such as the critical value $\Delta_{\rm crit}$ and the distribution of Δ:

- We assume that the IGM is in the local photo-ionization-recombination equilibrium, as commonly adopted (see, e.g., Fan et al. 2002); that is, the photoionization rate $n_{\rm HI}\Gamma$ is balanced by the recombination rate $n_{\rm HII}n_{\rm e}\alpha_{\rm B}(T)$, where $n_{\rm HI}$, $n_{\rm HII}$, and $n_{\rm e}$ are the proper number densities of neutral hydrogen, ionized hydrogen and electrons in the IGM, respectively, Γ is the number of photoionizations per H atom per unit time and is roughly proportional to the ionizing photon emis-

sion rate, and $\alpha_{\rm B}(T)$ is the recombination coefficient at temperature T (Abel et al. 1997). Note that $\dot{N}^{\rm bias}_{\rm phs,star}(z_{\rm Q}\simeq 6.2-6.4)\simeq 2\bar{\dot{N}}_{\rm phs,star}(z\sim 5)$ and that the mean hydrogen density in the rare overdense regions associated with the highest redshift QSOs at $z_{\rm Q}$ is higher than the cosmic mean at $z\sim 5$ by the same factor of 2. Thus, compared to the photo-ionization equilibrium at $z\sim 5$, given the same ionization ratio of $n_{\rm HII}/n_{\rm HI}$, the effect of a higher ionizing photon emission rate at $z\sim 6.2$–6.4 is compensated by the effect of a higher hydrogen density in the rare overdense regions. Hence, we set the critical overdensity $\Delta_{\rm crit}$ within the rare overdense regions associated with the highest redshift QSOs at $z_{\rm Q}\sim 6.2-6.4$ to be similar to that in the cosmic average regions at $z\sim 5$. The cosmic average ionization state of the IGM at redshift $z\sim 5$ has been measured by Fan et al. (2002) through the high-redshift QSOs around that redshift and $\Delta_{\rm crit}\simeq 10-20$ (see Fig. 8 in Fan et al. 2002). The simple arguments above have circumvented a more sophisticated and lengthy way to obtain $\Delta_{\rm crit}$, i.e., using $\dot{N}^{\rm bias}_{\rm phs,star}(z_{\rm Q})$ and repeating some detailed formalisms used in Miralda-Escudé et al. (2000), which gives an even larger $\Delta_{\rm crit}$. Hereafter, we simply adopt $\Delta_{\rm crit}\simeq 10-20$. At least the regions with overdensity below this value can be highly ionized by stars. This value is also compatible with the constraint on the reionization process from the Strömgren sphere in § 4.

- Since the mass fraction of halos with mass greater than $M_{\rm min}$ within the rare overdense regions associated with the highest redshift QSOs is similar to the cosmic mean fraction at a later time $z\sim 4.5-4.8$ [see Fig. 1a, where $F_{\rm halo}(>M_4,z)\simeq 10 g_{\rm star}(z)$, or see Tab. 2], we assume that the volume-weighted mass density distribution of baryons outside of halos in these rare overdense regions is analogous to (or at least does not significantly deviate from) the cosmic mean distribution at a later time $z\sim 4.5-4.8$. Numerical simulations have shown that the cosmic mean volume-weighted density distribution function $P(\Delta)$, defined so that $P(\Delta)d\Delta$ represents the fraction of the volume occupied by regions with overdensity in the range $\Delta\rightarrow\Delta+d\Delta$, is described by (Miralda-Escudé et al. 2000)

$$P(\Delta)=A\exp\left[-\frac{(\Delta^{-2/3}-C_0)^2}{2(\delta_0/3)^2}\right]\Delta^{-\beta}, \qquad (19)$$

where A and C_0 are set by normalizing $\int P(\Delta)d\Delta=1$ and $\int\Delta P(\Delta)d\Delta=1$, and δ_0 and β are given by simulations, for example, $\delta_0=3$ and $\beta=2.41$ at $z\sim 5$, and $\delta_0=3.6$ and $\beta=2.25$ at $z\sim 4$ (Chiu et al. 2003). The $P(\Delta)$ given by simulations may be biased away from the reality because of the small size of the box adopted in numerical simulations (Barkana & Loeb 2004), but the bias is not much for the high redshift $z_{\rm Q}\sim 6.2-6.4$ considered in this paper.

Using the distribution $P(\Delta)$ given by numerical simulations at both $z\sim 4$ and $z\sim 5$ (eq. 19), we obtain that the mass fraction of baryons or hydrogen in the regions with overdensity $\Delta\lesssim\Delta_{\rm crit}\sim 10-20$ is about $x_{\rm H}(\Delta\lesssim\Delta_{\rm crit})=\int_0^{\sim 10-20}\Delta P(\Delta)d\Delta\sim 0.7-0.8$. Considering that the mass fraction of hydrogen in IGM is ~ 0.9 in the regions associated with the highest redshift QSOs as obtained in § 3.2 and that not only the IGM with low densities ($\Delta\lesssim\Delta_{\rm crit}\sim 10-20$) but also part of the IGM with high density ($\Delta\gtrsim\Delta_{\rm crit}$) may also be ionized by photons from stars, the neutral hydrogen fraction is $x_{\rm HI}\simeq x_{\rm H,IGM}-x_{\rm H}(\Delta\lesssim\Delta_{\rm crit})\lesssim 0.1-0.2$ in those rare overdense regions before the reionization due to the QSO becomes effective.

Not only the models of structure and star formation above suggest that a significant number of stars have formed in the early universe to contribute to the reionization, there also exists emerging observational evidence suggesting rapid star formation [with a rate of $\sim 3000\,{\rm M_\odot\,yr^{-1}}$, which corresponds to an ionizing photon emission rate of $(0.5-0.9)\times 10^{56}\,{\rm s^{-1}}$ if the photon escaping fraction $f_{\rm esc}\sim 0.1-0.2$] in the host galaxies of the highest redshift QSOs. For example, (1) the high infrared luminosity observed in one of the highest redshift QSOs, SDSS J1148+5251, suggests that a large amount of dust has already formed (Bertoldi et al. 2003), and (2) the optical study of SDSS J1030+0524 suggests the existence of super-solar metalicities in the highest redshift QSOs (Pentericci et al. 2002), which are also expected to be the result of rapid star formation (Walter et al. 2003). The very high star formation rate suggests that large elliptical galaxies or the host galaxies of those QSOs with masses of $10^{11}-10^{12}\,{\rm M_\odot}$ formed on a dynamical timescale of a few times $10^8\,{\rm yr}$, which is roughly consistent with current scenario of the simultaneous formation of both QSOs/massive black holes and elliptical galaxies. If the mass of a massive black hole in those QSOs is around a few $10^9\,{\rm M_\odot}$, as estimated by Willott et al. (2003), the mass ratio of black holes to their host galaxies is $\sim 10^{-2}-10^{-3}$, which is close to the ratio found in nearby massive black holes and galaxies (e.g., Kormendy & Gebhardt 2001; Magorrian et al. 1998).

3.4. *The clumping factor of the hydrogen ionized by QSO photons*

As discussed above, inhomogeneity or clumpiness of hydrogen may have a significant effect on the reionization process. We define a clumping factor $C_{\rm HII}\equiv\langle(n_{\rm HII,Q})^2\rangle/\langle n_{\rm H}\rangle^2$ to describe the small-scale clumpiness of the hydrogen ionized by QSO photons (not collisionally ionized in halos or ionized by stars), where $n_{\rm HII,Q}$ is the proper number density of the hydrogen ionized by QSO photons, and "$\langle\cdots\rangle$" represents the average over the volume of the considered region. Note that our definition of the clumping factor here is a little different from that conventionally defined as $\langle(n_{\rm H})^2\rangle/\langle n_{\rm H}\rangle^2$, since the effects of stars and QSOs on the reionization are isolated in this paper (see also eq. 26). In the regions with proper radius $r_{\rm HII}$ and overdensity $\bar{\delta}_{r_{\rm HII}}$ at redshift z, we have $\langle n_{\rm H}\rangle(z)=(1+\bar{\delta}_{r_{\rm HII}})(1+z)^3\bar{N}_{\rm H}$ and $\bar{N}_{\rm H}\simeq(1-3Y_{\rm He}/4)\bar{\rho}_{\rm b}/m_{\rm H}$, where helium is assumed to be singly ionized and its abundance $Y_{\rm He}=0.24$. To estimate $C_{\rm HII}$, we divide the IGM in these regions into three components and then consider the contribu-

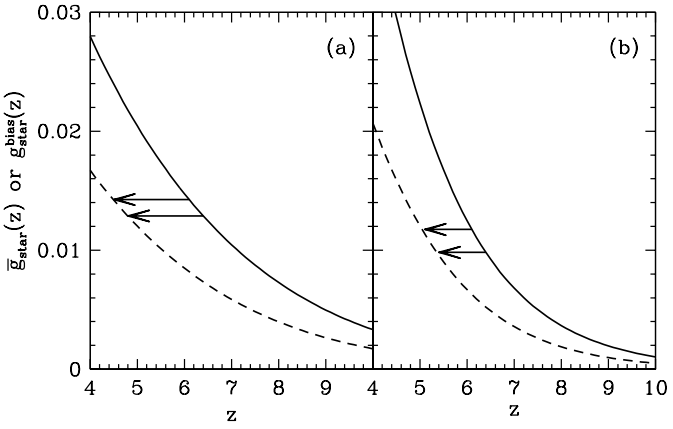

FIG. 1.— Mass fraction of baryons that are in formed stars as a function of redshift. The solid line represents the fraction for spheres with proper radius $r_{\rm Q} = 5\,{\rm Mpc}$ centering on the highest redshift QSOs [$g^{\rm bias}_{\rm star}(z)$; eq. 16], while the dashed line represents the cosmic mean fraction [$\bar{g}_{\rm star}(z)$; eq. 17]. Panels (a) and (b) show the results obtained from different star formation models (a) and (b) (described in § 3.3), respectively. As seen from this figure, although the mass fractions obtained from the two models are not exactly the same, $g^{\rm bias}_{\rm star}(z_{\rm Q} \sim 6.2-6.4)$ approaches the cosmic mean value $\bar{g}_{\rm star}(z)$ of a later time $z \sim 5$ in both models (indicated by the arrows). See details in § 3.3.

tion by each one: (i) Gas in subregions with overdensity $\Delta \lesssim \Delta_{\rm crit} \sim 10-20$, which has already been fully ionized by photons emitted from stars, as argued in § 3.3. This component is not responsible for the absorption of the QSO ionizing photons, and thus does not contribute to the clumping factor defined above. (ii) The remaining neutral gas in halos with mass greater than $M_{\rm min}$ (see the definition of $M_{\rm min}$ in § 3.2), which has not yet been collisionally ionized and cannot be photoevaporated out of the halo gravitational potential well. (iii) Gas in the subregions with overdensity $\Delta \gtrsim 10-20$ but outside of halos with mass greater than $M_{\rm min}$, which has not yet been fully ionized by photons from stars. Below we estimate the contribution by components ii and iii.

For component ii, it is plausible to assume that the remaining neutral gas only in the outer layer of these halos is ionized by the photons emitted from stars, and most of the remaining neutral gas in component ii will be ionized by QSO photons. The average contribution of component ii to $C_{\rm HII}$ can be estimated by

$$C^{\rm ii}_{\rm HII} \simeq \frac{f_{\rm int}\Delta_{\rm vir}}{(1+\bar{\delta}_{\rm r_{HII}})^2} \times \int_{M_{\rm min}}^{\infty} (1-y_{\rm H})^2 \frac{M}{\bar{\rho}} \left[\frac{dN}{dM}\right]^{\rm bias} dM, \quad (20)$$

where $\Delta_{\rm vir} \simeq 178$ is the virial overdensity and $f_{\rm int}$ is a weight parameter for the distribution of gas density in halos and $f_{\rm int} \simeq 3.14$ if the halo has a nonsingular isothermal density profile with a core radius of $0.1 r_{\rm vir}$ (see details in § 4 and Appendix B in Benson et al. 2001). For spheres with proper radius $r_{\rm Q} = 5\,{\rm Mpc}$ centering on the highest redshift QSOs at $z_{\rm Q} \simeq 6.2-6.4$, we have the mean overdensity $\bar{\delta}_{r_{\rm HII}} = \bar{\delta}_{r_{\rm Q}} \simeq 0.25$ (see § 3.1). Using equations (11) and (20), we find that

$$C^{\rm ii}_{\rm HII} \simeq 15-16. \quad (21)$$

The major contributors to $C^{\rm ii}_{\rm HII}$ are halos with mass in the range $M_{\rm min}$–$3M_{\rm min}$ and correspond to at most a mass fraction of

$$\simeq \frac{1}{(1+\bar{\delta}_{\rm r_{HII}})} \times \int_{M_{\rm min}}^{\infty} (1-y_{\rm H}) \frac{M}{\bar{\rho}} \left[\frac{dN}{dM}\right]^{\rm bias} dM \sim 2\%, \quad (22)$$

of the total baryon. Our calculation also shows that the number of halos for ionizing photons emitted from the central QSO at a random direction to pass through within the scale of $r_{\rm Q} = 5\,{\rm Mpc}$ is on average one, which is not too small to apply the average clumping factor at a random line of sight obtained by equation (20) to the particular observed QSOs. However, for QSOs with lower luminosity (e.g., with ionizing photon emission rate of less than $10^{56}\ {\rm s}^{-1}$ at $z_{\rm Q} \sim 6.2-6.4$), we find that the ionizing photons from the QSO at a significant fraction of its lines of sight may not encounter any halo with mass greater than $M_{\rm min}$ within the Strömgren sphere (but the photons could be absorbed by component iii), and thus the value of $C^{\rm ii}_{\rm HII}$ will be an overestimate for the particular observed QSOs if they are just located on these lines of sight (see discussions in § 4.3).

Compared to component ii, the contribution of component iii to $C_{\rm HII}$ is not easy to obtain accurately since the distribution of the IGM outside of halos and the effects of the photoevaporation process on minihalos within the rare overdense regions around the highest redshift QSOs are less well understood. To get the contribution of component iii, we consider the regions with overdensity $70 > \Delta \gtrsim 10-20$ (the upper limit 70 is set by the local overdensity at the virial radius of a halo with a nonsingular isothermal density profile and core radius $0.1 r_{\rm vir}$). Using the distribution given by equation (19) at $z \sim 4-5$, the clumping factor due to gas in regions with overdensity between $\sim 10-20$ and 70 is

$$\sim \frac{1}{(1+\bar{\delta}_{r_{\rm HII}})} \int_{\sim 10-20}^{70} \Delta^2 P(\Delta) d\Delta \sim 2-3. \quad (23)$$

On the one hand, this value can only be taken as a lower limit since the numerical simulations used to obtain equation (19) do not resolve halos with mass $\lesssim 10^6\,{\rm M}_\odot$ and the clumpiness in these smaller scales may also contribute to $C_{\rm HII}$. On other hand, the clumping factor estimated above may be not significantly smaller than the reality, since most of the gas in halos with mass $\lesssim 10^6\,{\rm M}_\odot$, especially in small halos, would be easily photoevaporated (Barkana & Loeb 1999; Shapiro et al. 2004), and part of the gas in regions with overdensity between $\sim 10-20$ and 70 may actually be ionized by photons from stars.

Note that the contribution from equation (23) does not include the contribution due to minihalos with mass between $M_{\rm res}$ and $M_{\rm min}$, which are also parts of component iii. With a simple model of the photoevaporation process, Haiman et al. (2001) argued that these minihalos are potentially important sinks of ionizing photons. Using numerical simulations of gas dynamics and radiation transfer in minihalos, Shapiro et al. (2004) argued that at $z = 9$ it may take only about $(1-1.5)\times 10^8\,{\rm yr}$ to photoevaporate these minihalos by a source at a distance of 1 Mpc away and emitting ionizing photons at a rate of $10^{56}\,{\rm s}^{-1}$ (or equivalently, at a

distance of 10 kpc away and with emission rate $10^{52}\,\mathrm{s}^{-1}$), and thus the photoevaporation process may reduce the required number of ionizing photons to reionize these minihalos. Our calculations in § 3.3 show that the average ionizing photons emitted from stars or galaxies at a distance of 1 Mpc from those minihalos is about $(0.5-1.1)\times10^{57}(1\,\mathrm{Mpc}/r)^2\,\mathrm{s}^{-1}\simeq(0.2-0.4)\times10^{56}\,\mathrm{s}^{-1}$ for model a and $(0.8-1.6)\times10^{57}(1\,\mathrm{Mpc}/r)^2\,\mathrm{s}^{-1}\simeq(0.3-0.6)\times10^{56}\,\mathrm{s}^{-1}$ for model b, respectively. These rates are significantly lower than the required rate given by Shapiro et al. (2004) to evaporate the gas in minihalos within a period of $(1-1.5)\times10^8$ yr. Therefore before the nuclear activity of the QSO turns on, despite that much of the gas in minihalos may have already been ionized and pushed out of the halo gravitational potential wells by the ionizing photons from stars, there should still remain a considerable fraction of gas in minihalos. After the nuclear activity turns on, the remaining gas will be ionized by QSO photons. As will be discussed in § 4, the time during which the QSO has radiated around the observed luminosity $\dot{N}^0_{\rm phs,Q}$ before the cosmic time $t(z_{\rm Q})$ is probably at most a few times 10^7 yr, which is shorter than the period $(1-1.5)\times10^8$ yr above; thus not all of the gas is evaporated at $z\sim z_{\rm Q}$. Using the static approximation of the photoevaporation process in minihalos, Barkana & Loeb (1999) show that a significant fraction of the gas (about 20%-40% for a typical QSO spectrum at redshift $z\sim8-20$) of big mini-halos ($\geq10^6\,\mathrm{M}_\odot$) is still gravitationally bounded to the potential well after the reionization of the universe is completed. Based on the tendency of the fraction with redshift shown in Barkana & Loeb (1999), this fraction could be larger at a lower redshift $z_{\rm Q}\sim6.2-6.4$. Below we simply assume that half of the gas still remains in minihalos and obtain the contribution of the minihalos to the clumping factor as follows:

$$0.5\times\frac{f_{\rm int}\Delta_{\rm vir}}{(1+\bar{\delta}_{\rm rHII})^2}\int_{M_{\rm res}}^{M_{\rm min}}\frac{M}{\bar{\rho}}\left[\frac{dN}{dM}\right]^{\rm bias}dM\simeq17-19. \quad (24)$$

Our calculation shows that within a proper scale of $r_{\rm Q}=5$ Mpc, the number of halos with mass between $M_{\rm res}$ and $M_{\rm min}$ passed by QSO photons at a random line of sight is on average $2-3$ before the photons are all absorbed, so that the average clumping factor obtained above can be applied to the specific observed QSOs. Our calculation also shows that the fraction of hydrogen remaining in the minihalos is

$$0.5\times\frac{1}{(1+\bar{\delta}_{\rm rHII})}\int_{M_{\rm res}}^{M_{\rm min}}\frac{M}{\bar{\rho}}\left[\frac{dN}{dM}\right]^{\rm bias}dM\simeq3\%. \quad (25)$$

Combining the contributions from components ii and iii, the clumping factor in the spheres considered in this paper (with $r_{\rm Q}=5$ Mpc at $z\sim6$) is

$$C_{\rm HII}=C^{\rm ii}_{\rm HII}+C^{\rm iii}_{\rm HII}\sim(34-38).$$

To more accurately estimate the clumping factor would require very high resolution numerical simulations with sufficiently large volume and incorporating dynamical effects of photo-evaporation and radiation transfer and simultaneous consideration of the ionizing effects from both stars and QSOs. The clumping factor $C_{\rm HII}$ may slowly decrease with time elapse because of the evolution of the gas density distribution (e.g., due to photoevaporation of some minihalos). Also, the distribution of (mini)halos within the Strömgren sphere is likely to be nonuniformly clustered and could further introduce fluctuations in $C_{\rm HII}$ for different lines of sight. In § 4 we shall use not only the estimate above but also some other different values of the clumping factor to illustrate the results.

4. THE EVOLUTION OF THE STRÖMGREN SPHERES AROUND THE HIGHEST REDSHIFT QSOS

4.1. *Models*

After the nuclear activity of the highest redshift QSO turns on, the neutral hydrogen remaining in high-density regions not ionized by stars will be further ionized by QSO photons and thus the neutral hydrogen fraction in the IGM surrounding the QSO will decrease. A spherical ionization front centering on the QSO will appear, separating the inside highly ionized HII region (due to QSO photons) and the outside partly ionized region (due to stars). The expansion of the apparent radius of the ionization front detected by observers (or the Strömgren radius; see the apparent shape of the Strömgren sphere in Yu 2004), $r_{\rm HII}$, can be described by the following equation for the number of hydrogen atoms ionized by the QSO in the Strömgren sphere:

$$\frac{4\pi}{3}\frac{d(x_{\rm HI}\langle n_{\rm H}\rangle r^3_{\rm HII})}{d\tau}=\dot{N}_{\rm phs,Q}(\tau)-\frac{4\pi}{3}\alpha_{\rm B}C_{\rm HII}\langle n_{\rm H}\rangle^2 r^3_{\rm HII}, \quad (26)$$

where $\tau=t-t_i$ is the time that the QSO has passed at cosmic time t since its nuclear activity was triggered at cosmic time t_i, $\dot{N}_{\rm phs,Q}(\tau)$ is the evolution of the QSO ionizing photon emission rate, and $\alpha_{\rm B}=2.6\times10^{-13}\,\mathrm{cm}^3\,\mathrm{s}^{-1}$ is the hydrogen recombination coefficient to excited levels of hydrogen at temperature $T=10^4$K (see Donahue & Shull 1987; Shapiro & Giroux 1987; Cen & Haiman 2000; Madau & Rees 2000; Yu 2004). The terms on the right-hand side of equation (26) account for the ionization due to QSO ionizing photons and the recombination within the Strömgren sphere, respectively. The role of the recombination can be characterized by a recombination timescale defined as follows:

$$\tau_{\rm rec}=x_{\rm HI}(C_{\rm HII}\langle n_{\rm H}\rangle\alpha_{\rm B})^{-1}\simeq4.8\times10^7\,\mathrm{yr}\frac{x_{\rm HI}}{(1+\bar{\delta}_{r_{\rm HII}})}\left(\frac{30}{C_{\rm HII}}\right)\left(\frac{7.42}{1+z}\right)^3. \quad (27)$$

The recombination is negligible if $\tau\ll\tau_{\rm rec}$, while important if $\tau>\tau_{\rm rec}$.

In equation (26) the parameters $x_{\rm HI}$, $\langle n_{\rm H}\rangle$, and $C_{\rm HII}$ are the average values within the dense region around a QSO with radius $r_{\rm HII}$ at cosmic time t, and their changes during the time interval $r_{\rm HII}/c$ of the QSO photon propagation in the Strömgren sphere are assumed to be negligible. Their changes caused by the Hubble expansion are also negligible. For simplicity, we shall also neglect their dependence on $r_{\rm HII}$ in the calculations below and set them to be the values averaged within a fixed scale, e.g., $r_{\rm HII}=r_{\rm Q}$ at $z_{\rm Q}$, as analyzed in § 3. This simplification will not affect our conclusions.

For the evolution of the QSO ionizing photon emission rate $\dot{N}_{\rm phs,Q}$, below we assume two simple models: in model i $\dot{N}_{\rm phs,Q} = \dot{N}^0_{\rm phs,Q}$ is constant, and in model ii $\dot{N}_{\rm phs,Q}$ increases with time exponentially, i.e., $\dot{N}_{\rm phs,Q}(\tau) = \dot{N}^0_{\rm phs,Q} \exp[(\tau - \tau_{\rm Q})/\tau_S]$ $(0 < \tau \leq \tau_{\rm Q})$, where $\tau_{\rm Q} = t(z_{\rm Q}) - t_i$ is the age of the QSO at $z_{\rm Q}$, $\tau_S \simeq 4.5 \times 10^7\,{\rm yr}[\epsilon/0.1(1-\epsilon)]$ is the Salpeter timescale, and ϵ is the mass-to-energy conversion efficiency and is ~ 0.1 (e.g., Gammie et al. 2004; Yu & Lu 2004a; Yu & Tremaine 2002). The ionizing photon emission rate is proportional to the QSO luminosity if their intrinsic continuum spectra do not differ significantly. Yu & Lu (2004a) show that the exponential increase of the QSO luminosity with a characteristic Salpeter timescale (that is, QSOs radiate at a rate close to their Eddington luminosity) appears to be generally consistent with the expected demographic relations between the QSO luminosity function and massive dormant black holes in nearby galaxies. It is likely that the luminosity evolution of a QSO also experiences a declining-luminosity phase (e.g, with the consumption of the accreting materials at the end of the nuclear activity), but this phase generally does not dominate the main population of luminous QSOs and is not considered in this paper, for simplicity (Yu & Lu 2004a). Models i and ii are almost the same if $\tau_{\rm Q} \ll \tau_S$.

The highest redshift QSOs are also observationally suggested to be accreting at a rate $\dot{M}_{\rm BH}$ close to the Eddington limit (Willott et al. 2003). With this observational constraint, in model i, the QSO age $\tau_{\rm Q}$ should be not longer than $M_{\rm BH}/\dot{M}_{\rm BH} \sim \tau_S$ (for this reason we extend the $\tau_{\rm Q}$-axis in Fig. 2a at most to a few times $10^7\,{\rm yr}$, rather than to $10^8\,{\rm yr}$ shown in Fig. 2b), and the cumulative ionizing photons emitted from the central QSO are at most 1-2 per hydrogen atom in the IGM within their Strömgren spheres (if $\epsilon \sim 0.1$), which is significantly less than those from stars (see § 3.3). Although in model ii $\tau_{\rm Q}$ may be much longer than τ_S, before $t(z_{\rm Q})$ most ionizing photons are emitted within the period from $t(z_{\rm Q}) - \tau_S$ to $t(z_{\rm Q})$. The time interval τ_S corresponds to a redshift interval of $\delta z \sim 0.3$ at $z_{\rm Q} \sim 6.2 - 6.4$. Cumulatively, most ionizing photons from stars before $t(z_{\rm Q})$ are emitted before $t(z_{\rm Q}+\delta z)$, and before $t(z_{\rm Q}+\delta z)$ most ionizing photons are not from QSOs but stars (see Fig. 1), which helps to justify the isolation of the ionization effect due to stars and that due to QSOs done in this paper (i.e., first consider stars and then QSOs).

Depending on whether the QSO shining time $\tau_{\rm Q}$ is much shorter than the recombination timescale $\tau_{\rm rec}$ (and the Salpeter timescale τ_S for model ii of $\dot{N}_{\rm phs,Q}$), equation (26) and its solution can be simplified into the following two cases:

- Case (1): if $\tau_{\rm Q} \ll \tau_{\rm rec}$ (and $\tau_{\rm Q} \ll \tau_S$ for model ii of $\dot{N}_{\rm phs,Q}$), the recombination term in equation (26) is negligible and the apparent size of the highly ionized HII region at $\tau = \tau_{\rm Q}$ is given by

$$r^0_{\rm HII} \simeq \left(\frac{3\int_0^{\tau_{\rm Q}} \dot{N}_{\rm phs,Q}(\tau) d\tau}{4\pi x_{\rm HI} \langle n_{\rm H} \rangle} \right)^{1/3}, \quad (28)$$

$$\simeq \left(\frac{3\dot{N}^0_{\rm phs,Q}\tau_{\rm Q}}{4\pi x_{\rm HI} \langle n_{\rm H} \rangle} \right)^{1/3}. \quad (29)$$

  In this case, given $\dot{N}^0_{\rm phs,Q}$ and $\langle n_H \rangle$, the size of $r^0_{\rm HII} \propto (\tau_{\rm Q}/x_{\rm HI})^{1/3}$ depends on the QSO age $\tau_{\rm Q}$ as well as the neutral hydrogen fraction $x_{\rm HI}$. There is little difference in the results from models i and ii.

- Case (2): if $\tau_{\rm Q} \gg \tau_{\rm rec}$, the recombination within the highly ionized HII region is approximately balanced by the emission of the ionizing photons from the QSO, and we have

$$r^0_{\rm HII} \simeq \left(\frac{3\dot{N}^0_{\rm phs,Q}\tau_{\rm rec}}{4\pi x_{\rm HI} \langle n_{\rm H} \rangle} \right)^{1/3},$$

$$= \left(\frac{3\dot{N}^0_{\rm phs,Q}}{4\pi \alpha_{\rm B} C_{\rm HII} \langle n_{\rm H} \rangle^2} \right)^{1/3} \equiv r_S \quad (30)$$

  for model i and

$$r^0_{\rm HII} \simeq \left(\frac{\tau_S}{\tau_{\rm rec} + \tau_S} \right)^{1/3} r_S \quad (31)$$

  for model ii. The definition of r_S above is similar to the classical formula of the Strömgren radius in stellar astronomy. In this case, given $\dot{N}^0_{\rm phs,Q}$ and $\langle n_H \rangle$, $r^0_{\rm HII}$ does not depend on the exact value of the QSO age $\tau_{\rm Q}$. If $\tau_S \gg \tau_{\rm rec}$ in model ii, there is little difference in the results of the two models and $r^0_{\rm HII}(\propto C_{\rm HII}^{-1/3})$ increases with decreasing $C_{\rm HII}$. The dependence of $C_{\rm HII}$ on $x_{\rm HI}$ is probably weak since most hydrogen atoms are actually located in low-density regions, while $C_{\rm HII}$ is mainly determined by the hydrogen in high-density regions (as illustrated in Fig. 2 in Miralda-Escudé et al. 2000). If $\tau_S \ll \tau_{\rm rec}$ in model ii, $r^0_{\rm HII}$ obtained from model ii is smaller than that from model i, and $r^0_{\rm HII}(\propto x_{\rm HI}^{-1/3})$ depends mainly on $x_{\rm HI}$ in model ii instead of $C_{\rm HII}$ in model i.

Below using the $\dot{N}_{\rm phs,Q}$ given by models i and ii, we solve equation (26) to illustrate the general properties of the evolution of $r_{\rm HII}$ by artificially setting different values for the clumping factor $C_{\rm HII}$ and the neutral hydrogen fraction $x_{\rm HI}$. The solutions of $r^0_{\rm HII}$ are shown as a function of the assumed QSO age $\tau_{\rm Q}$ in Figure 2. Panels (a) and (b) give the results for models i and ii of $\dot{N}_{\rm phs,Q}$, respectively. In both panels, the QSOs are assumed to be at $z_{\rm Q} = 6.3$ and have $\dot{N}^0_{\rm phs,Q} = 10^{57}{\rm erg\ s^{-1}}$, and we set $\bar{\delta}_{r_{\rm HII}} \simeq 0.25$, $C_{\rm HII}$=10, 30, and 50 (*dotted, dashed, and solid lines, respectively*), and $x_{\rm HI} = 10^{-2}, 10^{-1.5}, 10^{-1}, 10^{-0.5}$, and 1 (top to bottom for each line type). As seen from both panels, at the short-age end (e.g., $< 10^7\,{\rm yr}$), $r^0_{\rm HII}$ increases with increasing $\tau_{\rm Q}$ and decreasing $x_{\rm HI}$ as described by case 1 above in which the effect of recombination is insignificant (see eq. 29); while at the long-age end, with increasing QSO ages, $r^0_{\rm HII}$ roughly approaches a constant and the constant increases with decreasing $C_{\rm HII}$ as described by case 2. Given $C_{\rm HII}$, the value of the constant is generally independent of $x_{\rm HI}$ but may decrease with increasing $x_{\rm HI}$ if $x_{\rm HI}$ is sufficiently large (close to 1 so that $\tau_S \lesssim \tau_{\rm rec}$) in Figure 2b for model ii (see eqs. 30 and 31).

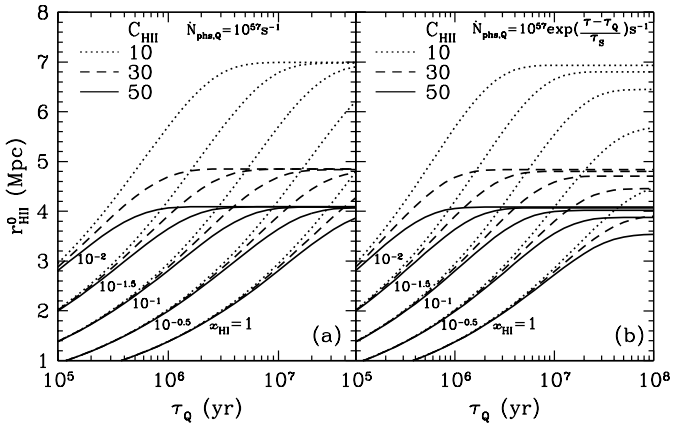

FIG. 2.— The expected apparent size of the Strömgren sphere $r^0_{\rm HII}$ as a function of the QSO age $\tau_{\rm Q}$. The QSOs are assumed to be at redshift $z_{\rm Q} = 6.3$. Different line types represent different clumping factors used (dotted, dashed, and solid lines for $C_{\rm HII}$ =10, 30, and 50, respectively). For each line type, we set the neutral hydrogen fraction $x_{\rm HI} = 10^{-2}, 10^{-1.5}, 10^{-1}, 10^{-0.5}$, and 1 from top to bottom. Panels (a) and (b) are for different models of the evolution of the QSO ionizing photon emission rate $\dot{N}_{\rm phs,Q}$ (models i and ii in § 4.1, respectively). As seen from this figure, if $\tau_{\rm Q}$ is significantly short, $r^0_{\rm HII}$ increases with increasing $\tau_{\rm Q}$ and decreasing $x_{\rm HI}$ (see eq. 27). If $\tau_{\rm Q}$ is long enough (e.g., $> 10^7$ yr), $r^0_{\rm HII}$ approaches a constant, independent of the detailed values of $\tau_{\rm Q}$. The constant is insensitive to the exact values of $x_{\rm HI}$ and the evolution models of $\dot{N}_{\rm phs,Q}$ used and is mainly determined by the clumping factor (the highest redshift QSOs considered in this paper belongs to this case), unless $x_{\rm HI}$ is big enough (close to 1) in panel (b) (see eqs. 30 and 31). See details in § 4.1.

4.2. *Comparison with observations*

For the highest redshift QSOs considered in this paper ($\bar{\delta}_{r_{\rm HII}} \simeq \bar{\delta}_{r_{\rm Q}} \simeq 0.25$, $x_{\rm HI} \lesssim 0.1-0.2$, $C_{\rm HII} \sim 36$, $z_{\rm Q} \sim$6.2–6.4; see details in § 3.3 and § 3.4), the averaged recombination timescale of the hydrogen in their surrounding regions is about $\tau_{\rm rec} \lesssim 5\times10^6$ yr. Note that the average lifetime of the main population of QSOs (with comoving number density peaked at $z \sim$2–3) has been determined to be $\tau_{\rm life} \gtrsim 4\times10^7$ yr (Yu & Lu 2004a; Yu & Tremaine 2002, see also Martini 2004 for a review of the QSO lifetime). If the lifetimes of the highest redshift QSOs are also $\gtrsim 4\times10^7$ yr, the probability that their ages are shorter than $\tau_{\rm rec}$ is therefore only $\sim \tau_{\rm rec}/\tau_{\rm life} \lesssim 10\%$, and the ages of the majority of the observed highest redshift QSOs are more likely to be around or longer than a few times 10^7 yr, which is significantly longer than $\tau_{\rm rec}$.

Even without the constraints of the QSO lifetime from other methods and an accurate estimate of $C_{\rm HII}$, by establishing a statistical method relating the distribution of the observed Strömgren radii with the probability distribution of the ages of the observed QSOs (somewhat similar to the manipulations in Yu & Lu 2004a,b), one can still check or rule out the possibility of whether the lifetime of the highest redshift QSOs is shorter than $\tau_{\rm rec}$ or whether the solution of $r^0_{\rm HII}$ belongs to case 1. For example, the observational distribution of $(\langle n_{\rm H}\rangle/\dot{N}^0_{\rm phs,Q})^{-1/3} r^0_{\rm HII,obs}$ can be estimated from a sample of QSOs having Gunn-Peterson troughs. This distribution should be consistent with a constant if most of the $r^0_{\rm HII}$ solutions belong to case 2, and consistent with the distribution of $\tau_{\rm Q}^{1/3}$ obtained by a random choice of $\tau_{\rm Q}$ for each QSO if most of the $r^0_{\rm HII}$ solutions belong to case 1 and $x_{\rm HI}$ is irrelevant to $\tau_{\rm Q}$ and does not differ much for different QSOs in the sample. Our preliminary results of applying this statistical method to the three highest redshift QSOs with measured Strömgren radii (in Tab. 1) have shown that the possibility of $\tau_{\rm life} < \tau_{\rm rec}$ is less than 15%. For simplicity, the details of this method are not presented in this paper and will be deferred to future work with an increasing number of the detected highest redshift QSOs having Gunn-Peterson troughs.

We conclude here that for most highest redshift QSOs the solution of $r^0_{\rm HII}$ belongs to case 2 and is insensitive to the exact values of the QSO age. For the highest redshift QSOs, we also have $\tau_{\rm rec} \ll \tau_S$ (in model ii), and thus $r^0_{\rm HII}$ is also insensitive to the neutral hydrogen fraction and the detailed evolution models of $\dot{N}_{\rm phs,Q}$ (see eqs. 30 and 31). The $r^0_{\rm HII}$ value is mainly determined by the QSO ionizing photon emission rate $\dot{N}^0_{\rm phs,Q}$ and the clumping factor $C_{\rm HII}$. Below we simply show the result obtained from model i.

We plot $r^0_{\rm HII}$ as a function of the ionizing photon emission rate of QSOs $\dot{N}^0_{\rm phs,Q}$ in Figure 3a. The observationally determined Strömgren radii of three QSOs and their ionizing photon emission rates (see Tab. 1) are shown by filled circles. The model results obtained by setting $\bar{\delta}_{r_{\rm HII}} \simeq \bar{\delta}_{r_{\rm Q}} \simeq 0.25$, $C_{\rm HII} = 36$, and $x_{\rm HI} \lesssim 0.1-0.2$ are shown by the dotted and solid curves, and by an open circle (in the range of $r^0_{\rm HII} \sim 4.9-5.9$ Mpc) for the source SDSS J1048+4637, which does not have a measured Strömgren radius in the literature. The different solid lines are for QSOs at different redshifts ($z_{\rm Q} = 6.2$, 6.3, and 6.4; top to bottom). We also illustrate the effects of $C_{\rm HII}$ by showing the results obtained by three other values of $C_{\rm HII}$=20, 30, and 45 in Figure 3a (top, middle, and bottom dotted lines, respectively; $z_{\rm Q} = 6.3$). The relation between the model and observational results for the three QSOs are more explicitly shown in Figure 3b (see solid circles). As seen from Figure 3, the model results are remarkably consistent with observations, which supports that the lifetimes of the highest redshift QSOs are around or longer than a few times 10^7 yr, as is the lifetime of the main population of QSOs (e.g., Yu & Lu 2004a; Yu & Tremaine 2002). The remarkable consistency also supports that the observational sizes of the Strömgren spheres of the highest redshift QSOs can be self-consistently explained by the fact that they are located in rare overdense regions and that the neutral hydrogen fraction in these regions is in the range from several percent to 10%–20% (before considering the reionization due to QSO photons). A much smaller neutral hydrogen fraction (e.g., $\ll 3\%$) will not be consistent with the clumping factor used, since $C_{\rm HII} \sim 36$ implies that a significant fraction of the neutral hydrogen (see eq. 25) remains in (mini)halos (which was neither ionized by the ionizing photons from stars nor photo-evaporated out of the halos) and contributes to $C_{\rm HII}$ (see eq. 25). Unless $C_{\rm HII}$ is much smaller than the estimate in this paper (e.g., because of stronger photo-evaporation of baryons in minihalos), a much shorter QSO lifetime ($\ll 10^7$ yr) will not be consistent with the observations of $r^0_{\rm HII,obs}$ since $r^0_{\rm HII}$ decreases with decreasing $\tau_{\rm Q}$ at short-$\tau_{\rm Q}$ ends (see Fig. 2).

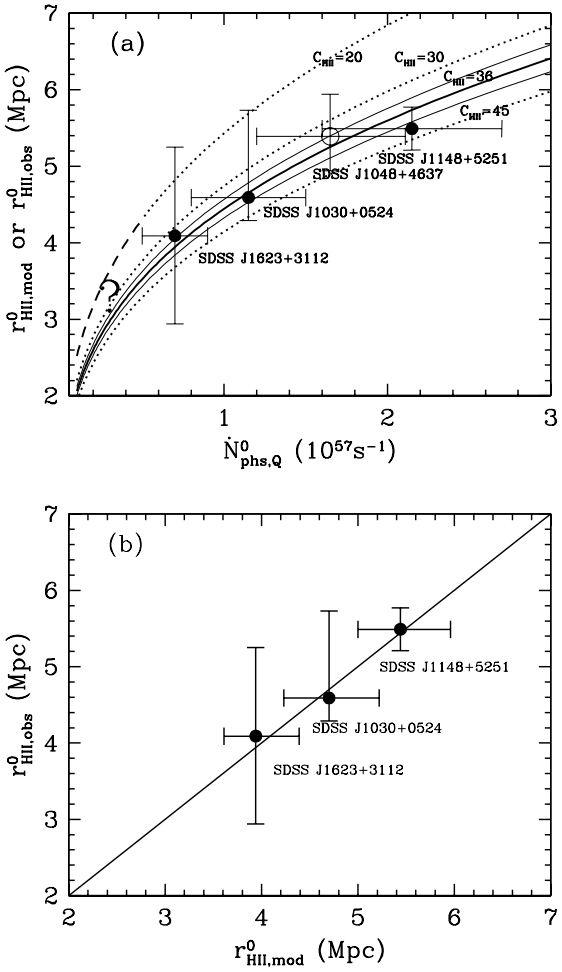

FIG. 3.— Panel (a): The size of the highly ionized HII regions $r^0_{\rm HII}$ of the highest redshift QSOs as a function of the ionizing photon emission rate $\dot{N}^0_{\rm phs,Q}$. The filled circles represent the observational data of the three QSOs with measured $r^0_{\rm HII,obs}$ given in the literature (see Tab. 1). The open circle gives our model results of $r^0_{\rm HII,mod}$ for the QSO J1048+4637 obtained by solving equation (26) and setting $\dot{N}^0_{\rm phs,Q}$ to be the mean of its upper and lower limits (listed in Table 1), and its estimated error bar in $r^0_{\rm HII,mod}$ represents the range of the upper and lower limits of $\dot{N}^0_{\rm phs,Q}$ (similarly for the model results of other sources shown in panel b). The dotted and solid curves also represent the model results. The dotted lines give the results for QSOs at $z_{\rm Q} = 6.3$, and the solid lines give the results for QSOs at $z_{\rm Q} = 6.2, 6.3, 6.4$ from top to bottom, respectively. The top and bottom dotted lines are obtained by setting $C_{\rm HII}$=20, 30 and 45, respectively; and the solid lines and the open circle are obtained by setting $C_{\rm HII} = 36$. Note that for low-luminosity QSOs (with $\dot{N}^0_{\rm phs,Q}$ smaller than a few times 10^{56} $\rm s^{-1}$) located in less dense regions, $C_{\rm HII} = 36$ could be an overestimate and the range of observed $r^0_{\rm HII}$ could be higher than those shown by the dotted and dashed lines and up to the dashed line (obtained by $C_{\rm HII} = 20$; see the region labeled by "?"). Panel (b): the model results of the apparent size of the Strömgren sphere $r^0_{\rm HII,mod}$ versus the size obtained from observations for the highest redshift QSOs $r^0_{\rm HII,obs}$ (solid circles). The solid line is a reference line. The remarkable consistency of the model results with observations supports that the observed Strömgren radii can be self-consistently explained by the dense environment around the highest redshift QSOs, the corresponding biased structure formation, star formation, and reionization processes analyzed in this paper, and the QSO lifetime longer than a few times 10^7 yr. If the observational $r^0_{\rm HII,obs}$ is systematically underestimated, then the realistic $C_{\rm HII}$ may be lower than ~ 36 and the photo-evaporation process in minihalos may be stronger than that assumed in this paper. See details in § 4.

The solution of $r^0_{\rm HII}$ in model ii is lower than that in model i by at most $1 - [\tau_S/(\tau_{\rm rec} + \tau_S)]^{1/3} \sim \tau_{\rm rec}/(3\tau_S)$. An independent constraint on the timescale τ_S may be obtained by comparing the result of model ii with the observation, as shown in Figure 3b, but this may require precise measurements of the observational Strömgren radius $r^0_{\rm HII,obs}$. The current observational error of $r^0_{\rm HII,obs}$ ($\delta r^0_{\rm HII,obs}$ ∼5%–30%; see Tab. 1) and the required consistency with the observation may give the constraint to be $\tau_S/\tau_{\rm rec} \gtrsim 1/(3\delta r^0_{\rm HII,obs})$ ∼1–7.

4.3. *Discussions*

The model results of $r^0_{\rm HII,mod}$ above are obtained by using the average clumping factor (over all the lines of sight). A significant contribution to the clumping factor comes from the neutral hydrogen in halos. In sparse regions, the ionizing photons may have been absorbed before they encounter any halo with mass greater than $M_{\rm min}$ at a significant fraction of the lines of sight. Thus the average contribution of component iii to $C_{\rm HII}$ may be an overestimate when applying it to a specific line of sight (see discussions in § 3.4). Hence, the model results above are usually appropriate to be applied to the observed high-luminosity QSOs located in dense regions, but are underestimates for low-luminosity QSOs (e.g., ionizing photon emission rate $\sim 10^{56}\,\rm s^{-1}$ at $z_{\rm Q}$ ∼6.2–6.4) located in less dense regions. The expected range of $r^0_{\rm HII}$ for low-luminosity QSOs can be estimated in the following way. By starting with their number density $N_{\rm Q}$ (obtained by extrapolating the luminosity function of the highest redshift QSOs with a power-law index of 3.2; see details in Fan et al. 2003, 2004) at the faint end and doing similar quantitative analysis for the environment around the low-luminosity QSOs as done for the high-luminosity QSOs above, we find that the clumping factor $C_{\rm HII}$ is around 40 for those lines of sight along which one halo with mass greater than $M_{\rm min}$ can be encountered within the Strömgren sphere, and around 20 for other lines of sight (e.g., 50% of all the lines of sight) along which no halo with mass greater than $M_{\rm min}$ is encountered (the details of the calculations are not given here for simplicity). Therefore, at a random line of sight, the size of the Strömgren spheres around the low-luminosity QSOs are roughly in the range of the results obtained by using $C_{\rm HII} \sim 20$ (dashed line in Fig. 3a) and $C_{\rm HII} \sim 36$ (see the region labeled by "?" between the dashed line and the solid lines in Fig. 3a). We believe that comparison of the range with future observations of the Strömgren radii of low-luminosity QSOs would further give some tests or constraints on the analysis or assumptions made in this paper, for example, on whether the major part of the clumping factor is due to the remaining neutral hydrogen in halos.

In addition, we note that a higher neutral hydrogen fraction ($x_{\rm HI} > 0.3$ if $\tau_{\rm Q} > 10^7$ yr) is obtained in Wyithe & Loeb (2004a), but it is obtained by using a much smaller clumping factor and without considering the detailed effects of the structure and star formation in the dense environment surrounding the highest redshift QSOs. Also, as mentioned in § 2 the Strömgren radius of SDSS 1030+0524 estimated by Mesinger & Haiman (2004) through the Lyβ trough in the QSO spectra ($\sim 6\,$Mpc) is larger than the value ($\sim 4.6\,$Mpc) listed

in Table 1. A possibly larger observational Strömgren radius may suggest that the realistic clumping factor for this QSO is smaller than the estimate in this paper (e.g., $C_{\rm HII}$ may be as low as ~ 20; see Fig. 2). A smaller $C_{\rm HII}$ may be caused by a stronger photoevaporation process in minihalos than that assumed in this paper. If more minihalos were photoevaporated, besides $C_{\rm HII}$, the neutral hydrogen fraction to be ionized by the central QSO, $x_{\rm HI}$, may also decrease. In short, most of the analysis in this paper will not be qualitatively affected even if the Strömgren radii estimated from current observations deviate slightly from reality.

As indicated in Figure 1, in the rare overdense regions around the highest redshift QSOs, the ionizing photon production per hydrogen atom in the IGM at $z \sim 7$ is already comparable to or higher than that of the cosmic average at $z \sim 6$ (when the reionization is complete). However, the reionization in the rare overdense regions around the highest redshift QSOs is not complete at a redshift significantly higher than $z_{\rm Q} \sim 6.2-6.4$ since neutral hydrogen must remain in the high-density regions to be ionized by QSO photons to satisfy the observational constraint from the Strömgren radius analyzed in this paper. The incomplete reionization in the overdense regions is partly caused by the fact that they have more high-density gas and that the gas is easier to recombine. This environmental effect has also been revealed in the numerical simulation by Ciardi et al. (2003), which shows that the reionization process in overdense regions may be complete at a time later than that in cosmic average regions, although the ionizing photon production per hydrogen atom in the IGM is higher in overdense environments than in cosmic average regions. According to this environmental effect revealed by Ciardi et al. (2003), the cosmic average neutral hydrogen fraction at $z \sim 6.2-6.4$ should be not higher than 10%–20% (the upper limit of $x_{\rm HI}$ surrounding the highest redshift QSOs). The observational flux upper limit of the Gunn-Peterson troughs has constrained the lower limit of the neutral hydrogen fraction (in mass) of the universe at $z \sim 6.2-6.4$ to be 1% (Fan et al. 2002). Therefore, the cosmic average neutral hydrogen fraction at $z \sim 6.2-6.4$ may be only a few percent. This low neutral hydrogen fraction alleviates the apparent conflict in reionization between the constraint from the highest redshift QSOs (e.g., Wyithe & Loeb 2004a) and that from the polarization spectrum of the cosmic microwave background (i.e., an early reionization at $z \sim 15$ or so; Kogut et al. 2003; Spergel et al. 2003).

5. CONCLUSIONS

In this paper we have investigated the dense environment, the reionization process, and the evolution of the Strömgren sphere around the highest redshift QSOs having Gunn-Peterson troughs ($z > 6.1$), and we have provided constraints on the intrinsic properties of QSOs and the reionization history of the universe by comparing the observed Strömgren radii with model results.

We have shown that the structure formation and consequently the gas distribution and star formation in the overdense regions around the highest redshift QSOs are biased from the cosmic average. Before the nuclear activity of the QSO turns on and its ionizing photon emission rate is high enough, the reionization in the overdense region surrounding the QSO is mainly contributed by stars, and starts from relatively low density subregions. Using some simple models of star formation and some analysis on the photoionization process inside and outside of halos (including minihalos), we have argued that a significant fraction of hydrogen in the Strömgren sphere around the QSOs is ionized by the ionizing photons from stars, and only about several percent to at most 10%–20% of hydrogen is left (e.g., in minihalos, halos, or high-density subregions) to be ionized by the QSO photons. The cosmic average neutral hydrogen fraction at $z \sim 6.2-6.4$ is also be smaller than the upper limit of 10%–20% obtained for the overdense regions and may be only a few percent, since overdense regions contain more high-density gas and are more difficult to reionize (Ciardi et al. 2003). We have analyzed the clumping property of hydrogen ionized by QSOs and studied the evolution of the apparent size of the Strömgren sphere. We have found that if the QSO lifetime is about or longer than a few times 10^7 yr, as is the lifetime of the main population of QSOs (with comoving number density peaked at $z \sim$2–3), the expected Strömgren radii from our models are very consistent with observations. With such a QSO lifetime, the ages of most of observed QSOs are long enough that the QSO photon emission is balanced by the recombination of the hydrogen ionized by QSOs in their Strömgren spheres, and the expected Strömgren radii from the balance are independent of the detailed values of the QSO ages. We also point out a statistical method involving a larger sample of highest redshift QSOs having Gunn-Peterson troughs in future observations, which may potentially check or rule out the possibility that the QSOs have a shorter lifetime (e.g., $< 10^7$ yr) even without an accurate estimate of the hydrogen clumping property.

We thank the referee for useful comments. Q.Y. acknowledges support provided by NASA through Hubble Fellowship grant #HF-01169.01-A awarded by the Space Telescope Science Institute, which is operated by the Association of Universities for Research in Astronomy, Inc., for NASA, under contract NAS 5-26555. Q.Y. acknowledges the hospitality of the Aspen Center for Physics, where part of this work was completed.

REFERENCES

Abel, T., Anninos, P., & Norman, M. L. 1997, New A, 2, 181
Abel, T., Bryan, G. L., & Norman, M. L. 2002, Science, 295, 93
Bajtlik, S., Duncan, R. C., & Ostriker, J. P. 1988, ApJ, 327, 570
Barkana, R. 2004, MNRAS, 347, 59
Barkana, R., & Loeb, A. 1999, ApJ, 523, 54
Barkana, R., & Loeb, A. 2001, Phys. Rep., 349, 125
Barkana, R., & Loeb, A. 2004, ApJ, 609, 474
Becker, R. H., et al. 2001, AJ, 122, 2850
Benson, A. J., Nusser, A., Sugiyama, N., & Lacey, C. G. 2001, MNRAS, 320, 153
Bertoldi, F., Carilli, C. L., Cox, P., Fan, X., Strauss, M. A., Beelen, A., Omont, A., & Zylka, R. 2003, A&A, 406, L55
Bond, J. R., Cole, S., Efstathiou, G., & Kaiser, N. 1991, ApJ, 379, 440
Bromm, V., Coppi, P. S., & Larson, R. B. 1999, ApJ, 527, L5
Cen, R. 2003a, ApJ, 591, 12
Cen, R. 2003b, ApJ, 597, 13
Cen, R., & Haiman, Z. 2000, ApJ, 542, L75
Chiu, W. A., Fan, X., & Ostriker, J. P. 2003, ApJ, 599, 759
Ciardi, B., Stoehr, F., & White, S. D. M. 2003, MNRAS, 343, 1101

TABLE 1. SAMPLE OF QSOS THAT HAVE THE GUNN-PETERSON TROUGH

Name	$z_{\rm Q}$	M_{1450}	$\dot{N}^0_{\rm phs,Q}$ (10^{57} s^{-1})	$z_{\rm HII,obs}$	$r^0_{\rm HII,obs}$ (Mpc)	$r^0_{\rm HII,mod}$ (Mpc)
SDSS J103027.10+052455.0	$6.28^{+0.02}_{-0.005}$	-27.15	$1.0^{+0.2}_{-0.2}$-$1.2^{+0.3}_{-0.2}$	6.20-6.28	$4.6^{+1.1}_{-0.3}$	4.2-5.2
SDSS J104845.05+463718.3	6.19±0.005	-27.55	$1.5^{+0.3}_{-0.3}$-$1.7^{+0.4}_{-0.3}$	··· -6.19	···	4.9-5.9
SDSS J114816.64+525150.3	6.42±0.005	-27.82	$1.9^{+0.4}_{-0.3}$-$2.2^{+0.5}_{-0.4}$	6.32-6.42	5.5±0.3	5.0-6.0
SDSS J162331.81+311200.5	6.22±0.02	-26.67	$0.6^{+0.2}_{-0.1}$-$0.7^{+0.2}_{-0.1}$	6.15-6.22	4.0±1.1	3.6-4.4

NOTE. — The $z_{\rm Q}$, M_{1450}, and $\dot{N}^0_{\rm phs,Q}$ are the redshift, absolute magnitude at 1450$\AA$, and ionizing photon emission rate of the QSOs. The $z_{\rm HII,obs}$ gives the range between the QSO redshift and the redshift of the onset of the Lyα Gunn-Peterson trough. The $r^0_{\rm HII,obs}$ gives the size of the Strömgren sphere that $z_{\rm HII,obs}$ corresponds to. For details about the observationally determined data and their errors, see § 2. The $r^0_{\rm HII,mod}$ is the Strömgren radius expected from the models in this paper (see also Fig. 3b).

Djorgovski, S. G., Castro, S., Stern, D., & Mahabal, A. A. 2001, ApJ, 560, 5L
Donahue, M., & Shull, J. M. 1987, ApJ, 323, L13
Eisenstein, D. J., & Hu, W. 1999, ApJ, 511, 5
Fan, X. et al. 2001, AJ, 122, 2833
Fan, X. et al. 2002, AJ, 123, 1247
Fan, X. et al. 2003, AJ, 125, 1649
Fan, X. et al. 2004, AJ, 128, 515
Furlanetto, S., Zaldarriaga, M., & Hernquist, L. 2004, ApJ, 613, 1
Gammie, C. F., Shapiro, S. L., & McKinney, J. C., 2004, ApJ, 602, 312
Gnedin, N. Y. 2000, ApJ, 535, 530
Gnedin, N. Y., & Prada, F. 2004, ApJ, 608, L77
Gunn, J. E., & Peterson, B. A. 1965, ApJ, 142, 1633
Haiman, Z., Abel, T., & Madau, P. 2001, ApJ, 551, 599
Haiman, Z., & Cen, R. 2002, ApJ, 578, 702
Haiman, Z., Rees, M. J., & Loeb, A. 1996, ApJ, 476, 458
Hernquist, L., & Springel, V. 2003, MNRAS, 341, 1253
Kauffmann, G, & Haehnelt, M. 2000, MNRAS, 318, L35
Kogut, A., et al. 2003, ApJS, 148, 161
Kormendy, J., & Gebhardt, K. 2001, in Wheeler J. C., Martel, H., eds, AIP Conf. Proc. Vol. 586, 20th Texas Symposium On Relativistic Astrophysics, Am. Inst. Phys., New York, p.363
Lacey, C., & Cole, S. 1993, MNRAS, 262, 627
Madau, P., Haardt, F., & Rees, M. J. 1999, ApJ, 514, 648
Madau, P., & Rees, M. J. 2000, ApJ, 542, L69
Magorrian, J., et al. 1998, AJ, 115, 2285
Maiolino, R., Schneider, R., Oliva, E., Bianchi, S., Ferrara, A., Mannucci, F., Pedani, M., & Roca Sogorb, M. 2004, Nature, 431, 533
Martini, P. 2004, Carnegie Observatories Astrophysics Series, Vol. 1: Coevolution of Black Holes and Galaxies, ed. L. C. Ho (Cambridge: Cambridge Univ. Press)
Mesinger, A., & Haiman, Z. 2004, ApJ, 611, L69
Mesinger, A., Haiman, Z., & Cen, R. 2004, ApJ, 613, 23
Miralda-Escudé, J. 1998, ApJ, 501, 15
Miralda-Escudé, J., Haehnelt, M., & Rees, M. J. 2000, ApJ, 530, 1
Mo, H., & White, S. D. M. 2002, MNRAS, 336, 112
Pentericci, L., et al. 2002, AJ, 123, 2151
Press, W. H., & Schechter, P. 1974, ApJ, 187, 425
Richards, G. T., Vanden Berk, D. E., Reichard, T. A., Hall, P. B., Schneider, D. P., SubbaRao, M., Thakar, A. R., & York, D. G. 2002, AJ, 124, 1
Santos, M. 2004, MNRAS, 349, 1137
Scalo, J. 1998, in ASP Conf. Ser. 142, The Stellar Initial Mass Function, ed. G. Gilmore & D. Howell (San Francisco: ASP), 201
Scheuer, P. 1965, Nature, 207, 963
Shapiro, P. R., & Giroux, M. L. 1987, ApJ, 321, L107
Shapiro, P. R., Iliev, I. T., & Raga, A. C. 2004, MNRAS, 348, 753
Sheth, R. K., & Tormen, G. 1999, MNRAS, 308, 119
Sheth, R. K., & Tormen, G. 2002, MNRAS, 329, 61
Sheth, R. K., Mo, H., & Tormen, G. 2001, MNRAS, 323, 1
Spergel, D. N., et al. 2003, ApJS, 148, 175
Sutherland, R., & Dopita, M. 1993, ApJS, 88, 253
Telfer, R. C., Zheng, W., Kriss, G. A., & Davidsen, A. F. 2002, ApJ, 565, 773
Walter, F., et al. 2003, Nature, 424, 406
White, R. L., Becker, R. H., Fan, X., & Strauss, M. A. 2003, AJ, 126, 1
White, S. D. M. 1994, Les Houches Lectures, astro-ph/9410043
Willott, C. J., McLure, R. J., & Jarvis, M. J. 2003, ApJ, 587, L15
Wyithe, J. S. B., & Loeb, A. 2004a, Nature, 427, 815
Wyithe, J. S. B., & Loeb, A. 2004b, astro-ph/0407162
Yu, Q. 2005, ApJ, in press, (astro-ph/0411097)
Yu, Q., & Lu, Y. 2004a, ApJ, 602, 603
Yu, Q., & Lu, Y. 2004b, ApJ, 610, 93
Yu, Q., & Tremaine, S. 2002, MNRAS, 335, 965

TABLE 2. MASS FRACTION OF BARYONS IN FORMED STARS AND IONIZING PHOTON EMISSION RATES FROM STARS

Model	$g_{\rm star}^{\rm bias}(z_{\rm Q})$ ($\times 10^{-2}$)	$\bar{g}_{\rm star}(z_{\rm Q})$ ($\times 10^{-2}$)	z $\bar{g}_{\rm star}(z) = g_{\rm star}^{\rm bias}(z_{\rm Q})$	$\dot{N}_{\rm phs,star}^{\rm bias}(z_{\rm Q})$ ($10^{57}\,{\rm s}^{-1}$)	$\bar{\dot{N}}_{\rm phs,star}(z\sim 5)$ ($10^{57}\,{\rm s}^{-1}$)
(a)	1.3-1.4	0.8	4.5-4.8	0.5-1.1	0.3-0.6
(b)	1.0-1.2	0.6	5.0-5.3	0.8-1.6	0.4-0.8

NOTE. — Models (a) and (b) are two different models for the star formation efficiency (i.e., the mass fraction of baryons to form stars) in halos (see details in § 3.3). The $\bar{g}_{\rm star}(z_{\rm Q})$ gives the mass fraction of baryons that are in formed stars in the rare overdense regions with proper radius $r_{\rm Q} = 5\,{\rm Mpc}$ around the highest redshift QSOs, where the QSO redshift $z_{\rm Q} \simeq 6.2 - 6.4$; and the $\bar{g}_{\rm star}(z_{\rm Q})$ gives the cosmic mean fraction at the same redshift. The fourth column gives the redshift at which $\bar{g}_{\rm star}(z) = g_{\rm star}^{\rm bias}(z_{\rm Q})$ (indicated by the arrows in Figure 1. The redshift is close to $z \sim 5$ for both models. The $\dot{N}_{\rm phs,star}^{\rm bias}(z_{\rm Q})$ gives the ionizing photon emission rates from stars in the overdense regions associated with the highest redshift QSOs at redshift $z_{\rm Q}$; and the $\bar{\dot{N}}_{\rm phs,star}(z\sim 5)$ gives the cosmic mean rate at $z \sim 5$. We have $\dot{N}_{\rm phs,star}^{\rm bias}(z_{\rm Q}) \simeq 2\bar{\dot{N}}_{\rm phs,star}(z\sim 5)$ for both models. See also Fig. 1 and § 3.3.